Marine Structures 82 (2022) 103147

Testing, simulation and design of offshore lined pipes under axial compression

Yidu Bu [a,b], Lu Yang [a], Zhenxing Zhu [a], Facheng Wang [b,*]

Keywords:
Axial compression
Corrosion resistance alloy (CRA)
Experiments
Lined pipe
Numerical modelling
Submarine pipeline

A B S T R A C T

As one of the means to inhibit offshore pipeline corrosion, lining a thin layer of stainless steel within the carbon steel pipeline provides an economical and durable design. Current design codes EN1993-1-1 and DNV–OS–F101 ignore the contribution of the liner pipes towards the cross-section capacity, which might lead to inefficient design. The focus of this study is to investigate the interaction of the two pipe layers arises during manufacture and the development of local buckling of the lined pipe under compression. Experiments to study the interaction behaviour of the liner pipe and the outer pipe, including saw tests and ring-split tests were performed. Then a series of short lined pipes were tested under axial compression, with a built-in camera to capture the development of liner wrinkling. After the tests, numerical models were developed and validated, and a series of parametric studies were conducted. The obtained test and FE results were used to assess the applicability of the codified provisions for the design of lined pipes under compression. Improved design method was developed considering the liner pipe contribution and material strain hardening. The proposed approach provides better prediction accuracies on the structural behaviours of lined pipes under axial compression.

1. Introduction

Offshore pipe lines made of carbon steel often develop internal corrosion when transmitting highly corrosive hydrocarbons. Lining internally a thin corrosion resistance alloy (CRA) layer within the carbon steel pipe can solve this problem. Lined pipes provide a more sustainable and durable design while keep the initial cost relatively low. The liners are usually bonded to outer pipes through either mechanical or thermal fabrication process and welded to the outer pipes at pipe ends [1,2]. The manufacturing process of lined pipes is shown in Fig. 1, where the liner pipe and the outer pipe are subjected to hoop stress and interact through the contact pressure.

Same as other submarine pipelines, lined pipes are exposed to plastic bending during offshore installation by Reel-lay method [3] and thermal compression during operation by transporting high temperature and high pressure (HTHP) hydrocarbons [4]. During operation the fault movements and ground subsidence can also cause compression in the pipes. Under significant deformation the liners can develop large wrinkles and buckle inwards and lead to undesirable local collapse accordingly [5,6]. Therefore, it is very important to study the interaction of the two layers under bending and compression, ensuring the two pipe layers are bonded together throughout installation and operation process.

There have been several studies on liner collapse development of lined pipes under bending both experimentally [7–11] and

Available online 21 December 2021
0951-8339/

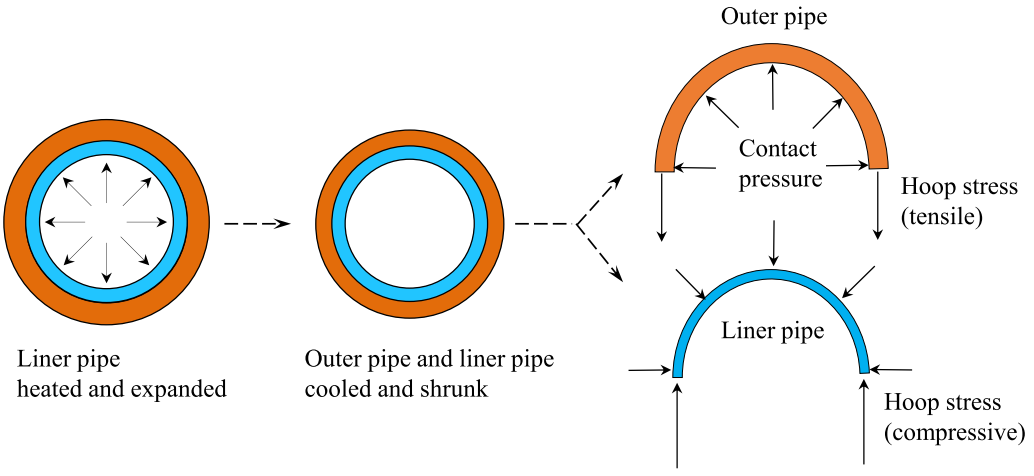

Fig. 1. Manufacturing process of lined pipes.

Table 1
Summary of tensile coupon material properties.

Coupon	Type	E (N/mm^2)	f_y (N/mm^2)	f_u (N/mm^2)	ε_f (%)
X65 Outer pipe-C	Curved	217,000	545	600	0.22
X65 Outer pipe-F	Flat	211,800	548	607	0.21
316L Liner-C	Curved	193,150	424	626	0.53
316L Liner-F	Flat	193,400	466	656	0.47

numerically [12–15] to evaluate the limits on the plastic bending of the liners. As both the outer and the liner pipes ovalize plastically under bending, the liner pipes may ovalize further and partially detach from the outer pipes and subsequently develop periodic wrinkles. The compressive behaviour of the lined pipes, however, has received much less attentions, where most of the research focuses on the numerical study of the liner wrinkling development. Yuan and Kyriakides [16] investigated the collapse mechanism of lined pipes under axial load numerically and found that the liner buckled at a relatively low strain then grew stably with compression and eventually collapsed at a higher strain. Jiao and Kyriakides [17] investigated tube specimens with mild wrinkles under persistent cycling and observed progressive growth of the amplitude of the pre-existing wrinkles, resulting in localized collapse of the tube under monotonic compression. Hilberink et al. [18] numerically studied the influence of variables on the interaction of the outer pipe ovalization and the liner piper wrinkling. Wang et al. [1] investigated the effects of key parameters on the ultimate strengths of lined pipes and proposed a confinement factor to ensure that the liner collapses after the outer pipe. There have been limited experimental investigations on lined pipes under axial compression. Focke et al. [19] planned two lined pipe tests under compression, unfortunately only one 10.750 inch TFP was successfully tested due to the limited capacity of the axial compression machine. More recently Bu et al. [2] studied the flexural buckling behaviour of the lined pipes experimentally on the member level. Though some studies have shown the outer-liner interaction, the contribution of the liner to the ultimate strength is usually ignored in engineering practice for a conservative concern [20].

This paper presents a systematic investigation of lined pipes under axial compression. Saw tests and ring-split tests were carried out to study the interaction between the two layers of pipes. Three short specimens were tested under compression and the wrinkling development of the liner were captured throughout the tests. Based on the test results, together with the supplementary numerical results, design codes EN 1993-1-1 [21] and DNV–OS–F101 [22] were evaluated. The predictions were found safely applicable to the design of lined pipe cross-sections, but overly conservative. A new design approach was developed to rationally consider the contributions of the liner component to the ultimate strength and to consider the material strain hardening, using the continuous strength method (CSM) [23,24]. The proposed method achieves better ultimate strength prediction accuracy for lined pipes under axial compression.

2. Lined pipe interaction behaviour

Prior to the stub column tests, three saw tests and three ring-split tests were carried out to study the interaction between the outer pipe and the liner pipe. All the tests and measurements were performed in the Laboratory Centre of Engineering Mechanics and Structural Engineering of the School of Civil Engineering at Shenyang Jianzhu University, China.

All the specimens in this section, together with the stub column specimens, were extracted from a commonly used type of lined pipe, which has a X65 carbon steel seamless outer pipe with 168.3 mm diameter and 12.7 mm wall thickness, lined with a 3.0 mm

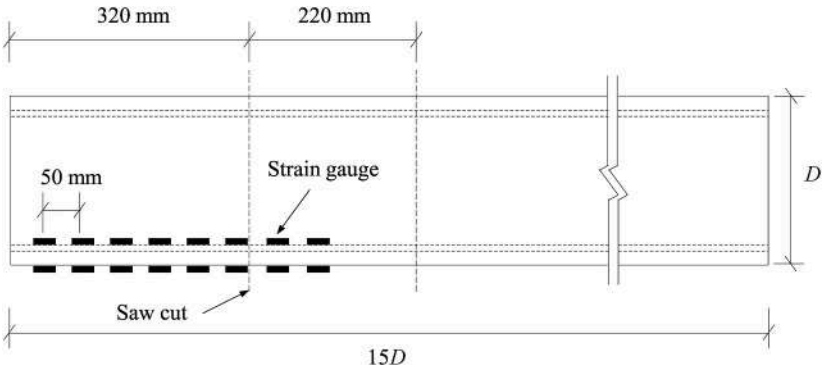

(a) Schematic drawing

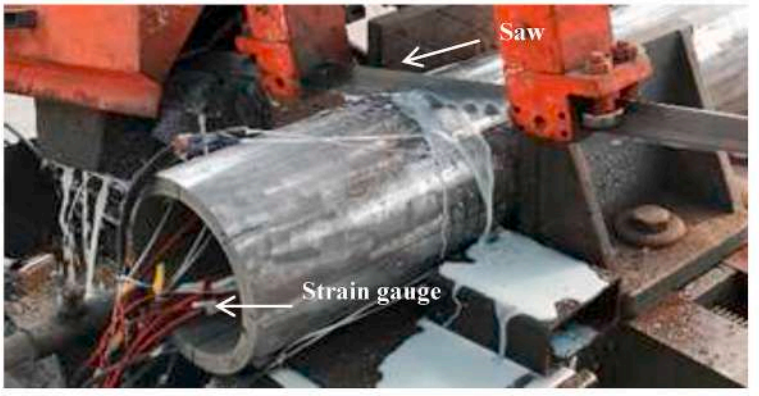

(b) Photo

Fig. 2. Saw test arrangement.

SS316L stainless steel liner pipe [25]. To simulate the practical service conditions, the specimens experienced reeling installation to 26 m water depth in Bohai Bay, China prior to the tests. Material tensile coupon tests were carried out by the authors in Ref. [2] and the key test results are summarized in Table 1, where "C" and "F" are appended to the specimen designation to indicate curved and flattened coupons, respectively, E is the Young's modulus, f_y and f_u are the yield or 0.2% proof strength and ultimate strength, and ε_f is the strain at fracture. The measured stress-strain responses for stainless steel were represented using the two-stage modified Ramberg-Osgood model [26] and the Ramberg-Osgood parameters n and $n_{0.2,1.0}$ are also listed in Table 1.

2.1. Saw tests

As show in Fig. 1, the bonding strength between the outer pipe and the liner pipe that arises during manufacture leads to the formation of initial axial stress. The magnitude of this axial bonding strength can be measured through saw tests. Measurements were made following the procedures recommended by the Specification for CRA clad or lined steel pipe [25]. Strain gauges were first attached to the inner and outer surfaces in pairs at 50 mm intervals along the longitudinal axis, then two cuttings perpendicular to the axial direction were conducted at 320 mm and 220 mm from the new edge of the specimen each time (Fig. 2). The changes in axial strains in both the liner and the outer pipe were recorded.

The absolute values of the axial strain results are given in Fig. 3. The measurements indicate that the changes in the axial strain were generally no more than 400 με and significantly less than lined pipes tested in a previous study [8,27], in which the saw tests were carried out prior to reeling. Since the specimen tested herein experienced a spooling-on and unloading process, there was a reduction on the bonding strength, which can be explained with the normality principle in plastic theory [28]. It is therefore suggested that the axial bonding strength of lined pipes after reeling installation is low and can be ignored when considering their structural integrity during operation.

2.2. Ring-split tests

In order to measure the residual hoop stress in lined pipes arises during the manufacturing process, ring split tests were carried out.

Three rings were cut from the remaining segment of the lined pipe in the saw tests. Each ring was perpendicularly cut to the axial direction of the pipeline at a width of 50 mm, following the recommendation in Ref. [27]. Four bi-axial strain gauges were placed

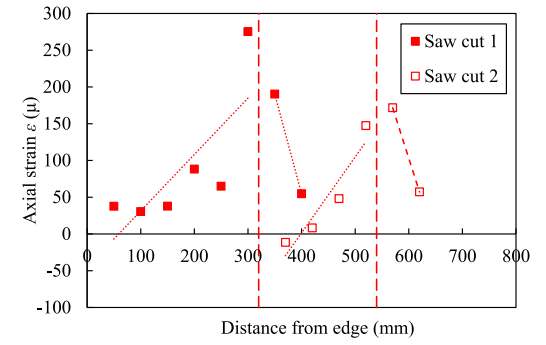

(a) Outer pipe

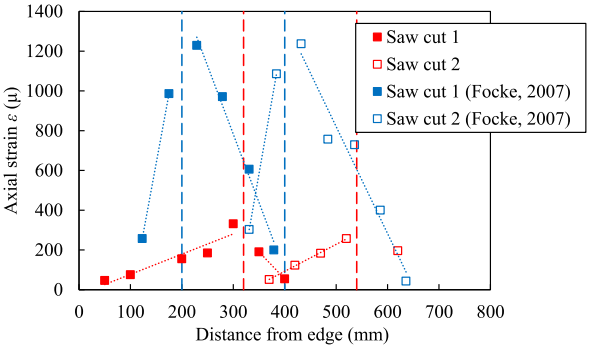

(b) Liner pipe

Fig. 3. Results of saw tests.

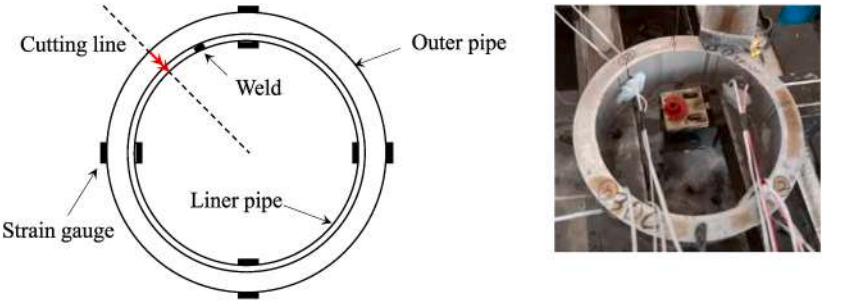

Fig. 4. Ring-split test arrangement.

circumferentially at the inner and the outer surface in pairs for each ring, as shown in Fig. 4. A two-step cut along the radial direction was then made on each ring by a DK7745 CNC wire cutting machine. The first cut was made through the thickness of the liner pipe. After the cut the specimen was free to expand radially and axially, and the initial hoop and axial stress were subsequently released. The bi-axial strain gauges recorded the radial and axial strain released after the readings were stable. The second cut was made along the same direction through the thickness of the liner pipe and the readings of the strain gauges were also recorded after they were stable. The average values of the changes in strains were used to calculate the released hoop and axial stress σ_h and σ_a according to a standard plane stress material law [6], as shown in Eqs. (1) and (2).

$$\sigma_h = \frac{E}{(1-\nu^2)} \cdot \left(\frac{\sum \varepsilon_h}{j} + \nu \frac{\sum \varepsilon_a}{j} \right) \tag{1}$$

$$\sigma_a = \frac{E}{(1-\nu^2)} \cdot \left(\frac{\sum \varepsilon_a}{j} + \nu \frac{\sum \varepsilon_h}{j} \right) \tag{2}$$

where ν is Poisson's ratio, j is the number of strain gauges, $\varepsilon_{h,o}$, $\varepsilon_{a,o}$, $\varepsilon_{h,i}$ and $\varepsilon_{a,i}$ are the average values of strain changes, with subscripts

Table 2
Results of ring-split tests.

Specimen	$\varepsilon_{h,o}$ (μ)	$\varepsilon_{a,o}$ (μ)	$\sigma_{h,o}$ (MPa)	$\sigma_{a,o}$ (MPa)	$\varepsilon_{h,i}$ (μ)	$\varepsilon_{a,i}$ (μ)	$\sigma_{h,i}$ (MPa)	$\sigma_{a,i}$ (MPa)
Ring 1 - outer split	−87	36	−18	2	61	21	14	8
Ring 1 - liner split	−90	36	−19	2	87	17	20	9
Ring 2 - outer split	−139	39	−30	−1	7	13	2	3
Ring 2 - liner split	−141	39	−31	−1	36	6	8	4
Ring 3 - outer split	−118	30	−26	−1	−2	31	2	6
Ring 3 - liner split	−120	30	−26	1	22	24	6	6

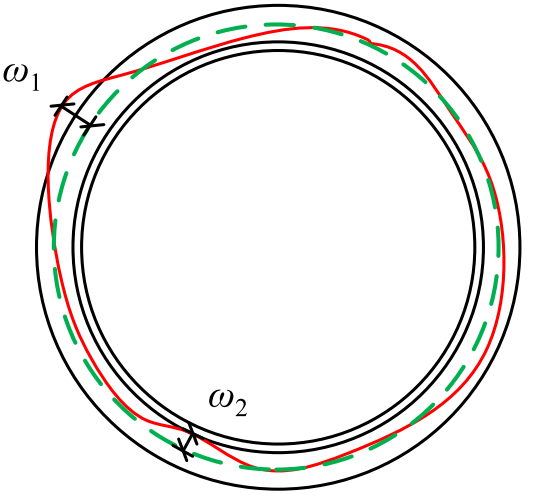

Fig. 5. Initial local imperfection.

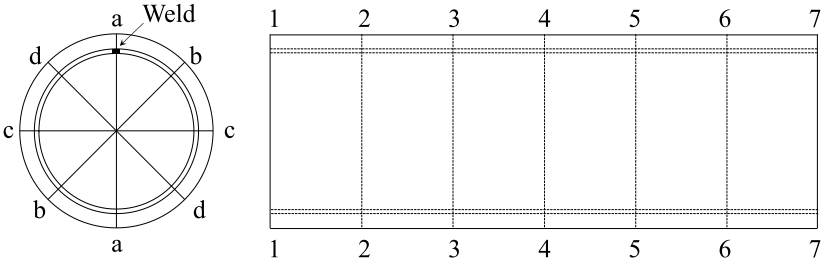

Fig. 6. Imperfection measurement locations.

"h" and "a" for hoop and axial and "o" and "i" for outer pipe and liner pipe, respectively. The average change in strains and calculated stresses are listed in Table 2. A positive strain value corresponds to a tensile strain, while negative corresponds to compressive strain. It can be seen that after the outer pipe was cut, the hoop strains of the outer pipe were negative, indicating that tensile strain existed in the outer pipe prior to the cutting and had been released. The average residual hoop stress released in the outer pipe was about 25 MPa. On the other hand, the liner pipe hoop strains were positive, indicating that the liner pipe was under compressive strain prior to the cutting. The average residual hoop stress released is about 6 MPa. This is consistent with the stress state of lined pipes after the manufacturing process shown in Fig. 1. When the liner was cut, because the strain in the outer pipe had been released, the hoop strain value remained unchanged; compressive hoop strains in the liner pipe increased for an equivalent hoop stress about 5 MPa. This is thought to be the release of residual hoop stress formed when the liner stainless steel pipe was welded.

3. Lined pipe axial compression tests

Three lined pipe ultimate strength tests were conducted to determine the cross-section load-carrying and deformation capacities under axial compression. The nominal length of the pipeline specimens was selected as 600 mm to be sufficiently long to include a representative distribution of local imperfections and at the same time to avoid global buckling. Both ends of each specimen were machined flat and welded to two 20 mm thick end plates with stiffeners.

Table 3
Measured geometries and imperfections of the short pipeline specimens.

Specimen	D_1 (mm)	D_2 (mm)	D_3 (mm)	D_4 (mm)	D_5 (mm)	D_6 (mm)	D_7 (mm)	L (mm)	t (mm)	Out-of-roundness (%)
LP-1	169.08	169.21	168.94	168.87	168.83	168.99	168.90	638.35	15.70	0.50%
LP-2	168.71	169.15	169.04	168.76	168.58	168.77	168.81	638.68	15.56	0.30%
LP-3	168.71	168.78	168.96	168.95	168.89	169.06	168.82	638.74	15.56	0.50%
Mean	168.83	169.05	168.98	168.86	168.77	168.94	168.84	638.59	15.61	0.43%

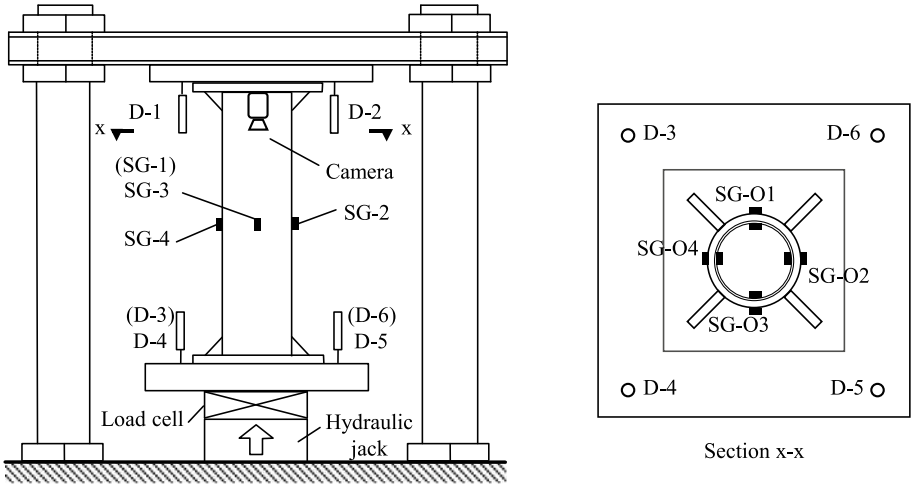

(a) Schematic drawing

(b) Photo

(c) End plate slit with camera

Fig. 7. Short lined pipe under axial compression test set-up.

Table 4
Summarized geometric properties and test results of the short pipelines.

Specimen	D_o (mm)	t (mm)	L (mm)	N_u (kN)	δ_u (mm)	ω_0 (mm)
LP-1	168.87	15.70	638.35	4490	21.4	0.4
LP-2	168.76	15.54	638.68	4651	26.5	0.3
LP-3	168.98	15.56	638.74	4551	13.9	0.4
Mean	168.87	15.60	638.59	4564	20.6	0.4

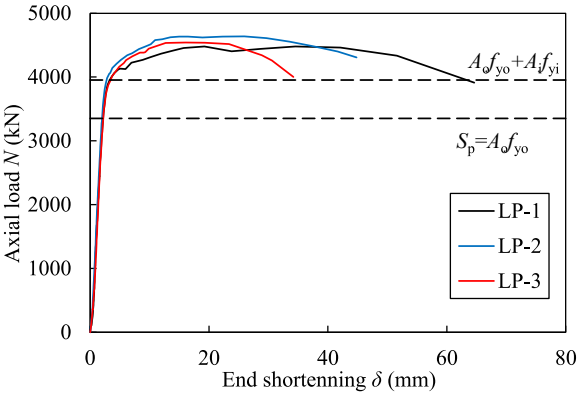

Fig. 8. Short lined pipe load-end shortening curves.

3.1. Geometry and imperfection measurements

Initial local geometric imperfections are the changes of wall thickness or radius of a cross-section of the pipe specimen in relate to the ideal pipe, as shown in Fig. 5. A vernier caliper with an accuracy of 0.02 mm was used to measure the out-of-roundness ratio of the specimens. The inner diameter was measured at four angles at both ends of the specimen (Cross-sections 1 and 7), while the outer diameter was measured at four angles at Cross-sections 1 to 7, as shown in Fig. 6. The average measurements are shown in Table 3, where D_n is the average outer diameter of Cross-section n, L is the average length the test piece with end plates, and t is the average difference between the outer and inner diameters of the pipe end. Out-of-roundness ratios were calculated as the maximum diameter minus the minimum diameter divided by the mean diameter and all the ratios were found to be within the 1% limit in API 5L [29].

3.2. Test setup and results

The stub column test setup is shown in Fig. 7, following the setup adopted in similar investigations [19,30,31]. A 5000 kN hydraulic testing machine was used, where all the short lined pipes were axially compressed using load control, at approximate rates of 100 kN/min. The full-histories of load, strain and ending shortening were recorded at 1 s interval, using Mobrey IMP acquisition equipment and DH3820 computer package.

Strain gauges were affixed at the mid-length of the specimen with the liner weld located centrally between the adjacent strain gauges in the longitudinal direction, where SG-O1 to SG-O4 and SG-L1 to SG-L4 represent strain gauges placed on the outside and inside of the pipe, respectively. Six displacement transducers were used to capture average end shortenings, marked as D1 to D6 in Fig. 7(a). The top end plate was designed with a T-shaped groove (Fig. 7(c)) to connect strain gauge wires from the inside of the pipe. A micro camera was also installed on the top end plate to capture the wrinkle development of the liner pipe.

The summarized geometric measurements and the key test results are listed in Table 4, where D_o is the average diameter, N_u is the ultimate strength, δ_u is the end shortening at the ultimate load.

The load-end shortening N–δ curves for all tested specimens are presented in Fig. 8, showing a good extend of strain hardening before failure. The resistances calculated according to DNV–OS–F101 [22] S_p and the yield load of the whole cross-section $A_o f_{yo} + A_i f_{yi}$, (A_o and A_i are the cross-sectional areas of the outer pipe and liner pipe, f_{yo} and f_{yi} are the yield strength of the outer pipe and the proof strength of the liner pipe) are outlined in Fig. 8, too. The current engineering practice generally determines the lined pipe compressive resistance by only considering the outer pipe for a conservative concern. The N–δ curves show greater load carrying capacities than the calculated resistances. This enhancement might be attributed to the contributions of the liners and significant strain hardening behaviour.

The load-strain N–ε curves from a typical specimen LP-3 are shown in Fig. 9, where the values of the compressive strain are used. At the initial stage of loading, the axial strains of the outer and liner pipes were at similar values, showing that the pipe cross-section was under uniform compression. Later in the loading stage, readings of some strain gauges had a kink, showing the wrinkle development

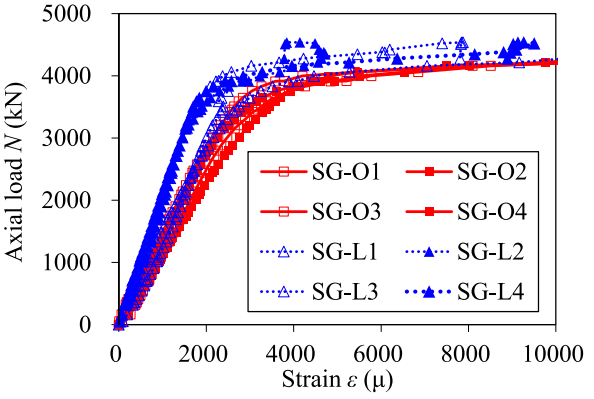

Fig. 9. Short lined pipe load-strain curves (Specimen LP-3).

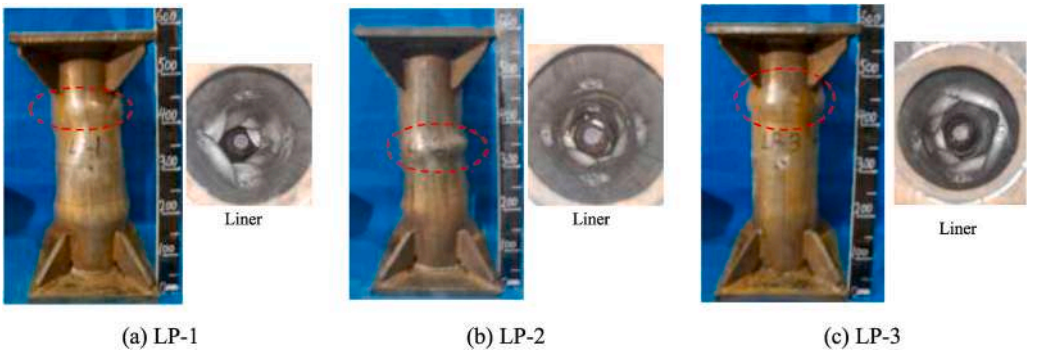

Fig. 10. Short lined pipe failure modes.

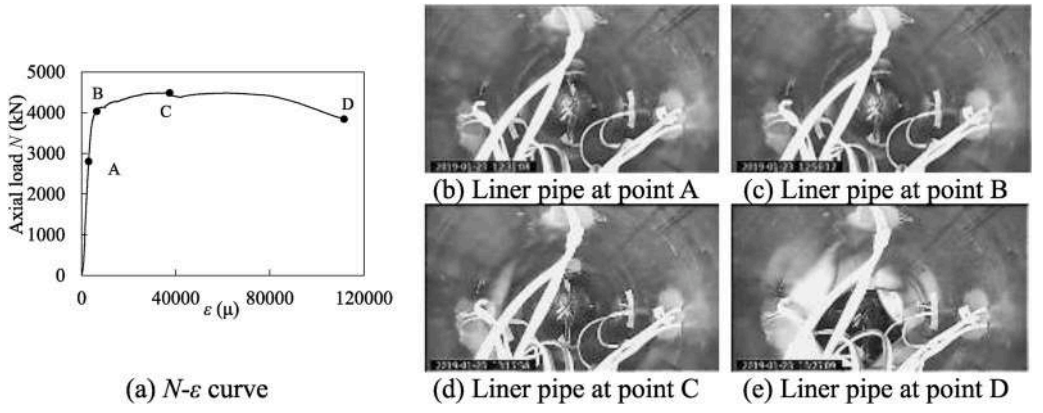

Fig. 11. Development of liner failure of specimen LP-1.

near those strain gauges.

All the tested specimens were observed with local buckling failure modes, as shown in Fig. 10, together with the failure mode from the inside of the pipe captured by the camera. In these three specimens local buckling initiated in different cross-sections due to local imperfections of different specimens. The liner failure development of each specimen was analysed through the load-average strain curves and liner wrinkle development, as shown in Figs. 11–13. Following the analysis in Ref. [1], the load-average strain curves of the tested specimens were divided by different stiffness values into four stages: elastic, elastic-plastic, plastic and declining.

Stage 1: Elastic (Point O-A). Load increased linearly and sharply with axial strain to around 60%N_u. Both components have similar Poisson's ratio and Young's modulus. However, as stainless steel has a rounded stress-strain behaviour with gradual reduction on the stiffness, while the carbon steel outer pipe stiffness remains the same in the elastic stage, this leads to increasingly larger

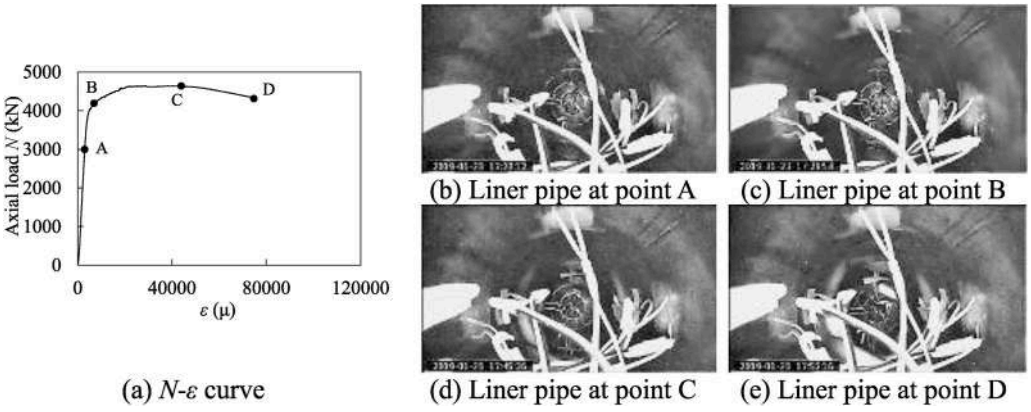

Fig. 12. Development of liner failure of specimen LP-2.

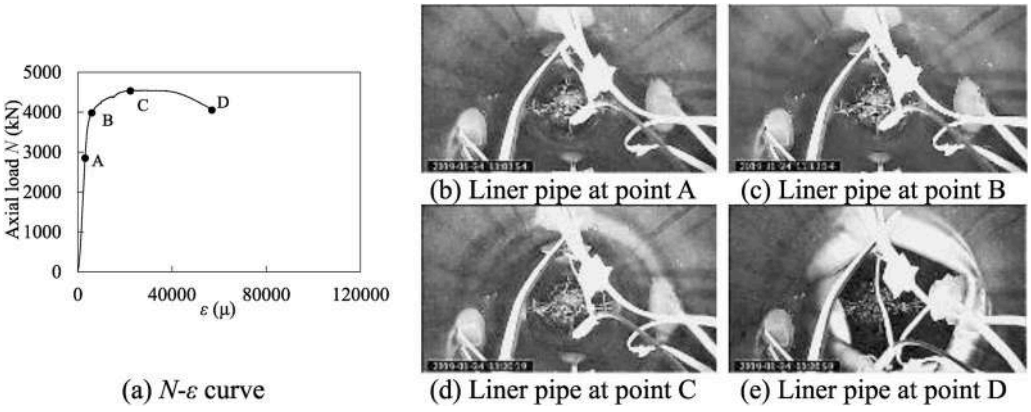

Fig. 13. Development of liner failure of specimen LP-3.

circumferential expansion of the liner pipe which is confined by the outer pipe. At this stage no buckling was observed.

Stage 2: Elastic-plastic (Point A-B). The stiffness of the N-ε curve gradually decreased due to material yielding. The decrease in stiffness was mainly from the outer pipe, as the material became perfectly plastic. The circumferential expansion of the outer pipe subsequently became larger than the liner. According to previous research [1], at the end of this stage, the outer pipe and the liner pipe bear axial compression independently with no interaction. No buckling was observed at this stage.

Stage 3: Plastic (Point B–C). The stiffness of the N-ε curve significantly decreased while the load increased to N_u. With the commonly stocky cross-sections, pipeline generally experience certain amount of axial strain without much further increase of the load due to both the yielding plateau of carbon steel outer pipe and the largely reduced tangential modulus of the stainless liner. This trend ended while the ultimate strength N_u has been approached, where the local buckling occurrence of pipe cross-section being observed. As the liner pipe was no longer confined by the outer pipe, local buckling initiated during this stage and can be clearly observed at the end of this stage.

Stage 4: Declining (Point C-D). The load became decreasing as the axial strain increased. The liner pipe developed into diamond-like shapes due the local buckling occurrence and the redistributions of the longitudinal stresses within the lined pipe cross-section caused the local buckling of the outer pipe, as illustrated in Fig. 16.

4. Numerical modelling

Numerical investigations into the behaviour of lined pipe cross-sections were carried out using the general-purpose finite element (FE) package ABAQUS [32]. The models were validated against the obtained stub column test results.

4.1. Modelling assumptions

Specimens were modelled with measured geometries and material properties, as listed in Tables 1 and 4, where the thickness of the outer pipe t_o and the liner pipe t_i were taken proportionally to the nominal thickness of the measured total thickness. The average measured engineering stress-strain responses were converted into true stress and log plastic strain and applied in the FE models,

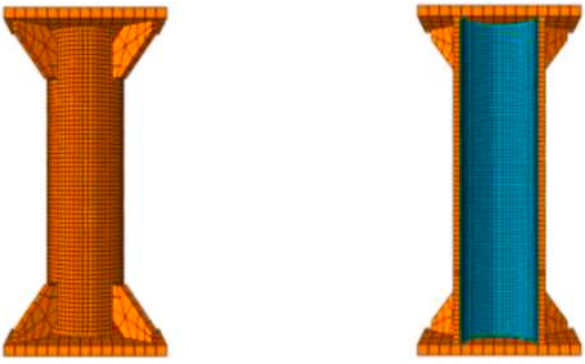

Fig. 14. Finite element model.

Table 5
Comparison of experimental and numerical results.

Specimen	k_{test} (kN)	k_{FE} (kN)	k_{test}/k_{FE}	N_{test}(kN)	N_{FE}(kN)	N_{test}/N_{FE}
LP-1	1,583,734	1,600,280	0.990	4490	4395	1.022
LP-2	1,597,872	1,614,472	0.990	4651	4662	0.997
LP-3	1,472,462	1,651,410	0.892	4551	4535	1.004
Mean			0.957			1.008
COV			0.059			0.013

following the method in Ref. [33]. Stiffeners and end plates were meshed with 3D solid elements C3D8R, while the liner pipe and the outer pipe were meshed with shell elements S4R. There have been several studies on the mesh size in stainless steel numerical simulations [34–36]. The mesh size along the circumferential and longitudinal directions of the sections was similar to the pipe thickness, following the same rule employed in a previous numerical study of lined pipes [2]. One element was assigned through thickness of both the outer pipe and the liner pipe and the mesh aspect ratio was taken close to one. All degrees of freedom for the nodes of the loaded end were restrained, apart from the longitudinal translation. A typical finite element mesh used in this study is shown in Fig. 14.

The residual axial stress and residual hoop stress generated from the fabrication process of lined pipes were measured in the saw tests and ring-split tests in Section 2. However, both were not considered in this study for the following reasons. Residual axial stress was not considered in the stub column models since the axial stress were released when the stub columns were cut out and the axial stress does not influence the cross-sectional behaviour. Residual hoop stress was not considered in the numerical models since the measured values are small. Previous numerical study conducted by Hilberink et al. [37] also shown that ignoring residual hoop stress still offers accurate results. Therefore, a snug-fit lined pipe with neither a radial contact stress nor a gap was modelled. Surface-to-surface with hard contact and finite sliding with no friction were applied between the two pipe layers, similar to Refs. [13, 37], where the outer pipe was set as the master surface and the liner pipe as the slave surface.

The previous study by Hilberink [37] investigated the wrinkling behaviour of lined pipe numerically. It was found that under axial compression, the liner pipe and the outer pipe initially deformed uniformly in radial direction until the liner started to exert an increased contact pressure on the inside of the outer pipe. Due to the contact between the two layers, the imperfection mode in this reference was not acquired from typical eigenvalue analyses. However, a sensitivity study [37] showed that the resulting wrinkle development were relatively insensitive to the initial imperfection shape introduced.

Therefore, in this study, the amplitude was taken from the back calculation of the measured out-of-roundness ratios, as listed in Table 4, while the imperfection mode was selected from eigenvalue analyses to match the failure mode obtained from the tests.

4.2. Validation of the numerical models

FE models of the three tested specimens were produced and validated against the test results. Table 5 lists the comparisons of the initial stiffness k_{test} and k_{FE}, the initial slope of linear part of the axial load – strain curve, and the ultimate capacity N_{test} and N_{FE}. The mean values and the coefficients of variation (COV) of the test/FE ratios show that the numerical models can provide accurate predictions of the behaviour in the physical tests. The load-end shortening curves are compared in Fig. 15. The full experimental load-end shortening response are accurately replicated. Fig. 16 shows the comparison of the test and FE failure modes of all stub column specimens from the outside and inside of the pipe. It can be seen from the figure that the typical failure mode of stub column lined pipes is that the outer pipe is locally bulging outwards while the liner pipe develops wrinkle inwards. The shapes and positions of the local buckling obtained by the numerical analysis are similar to those obtained by the experiments.

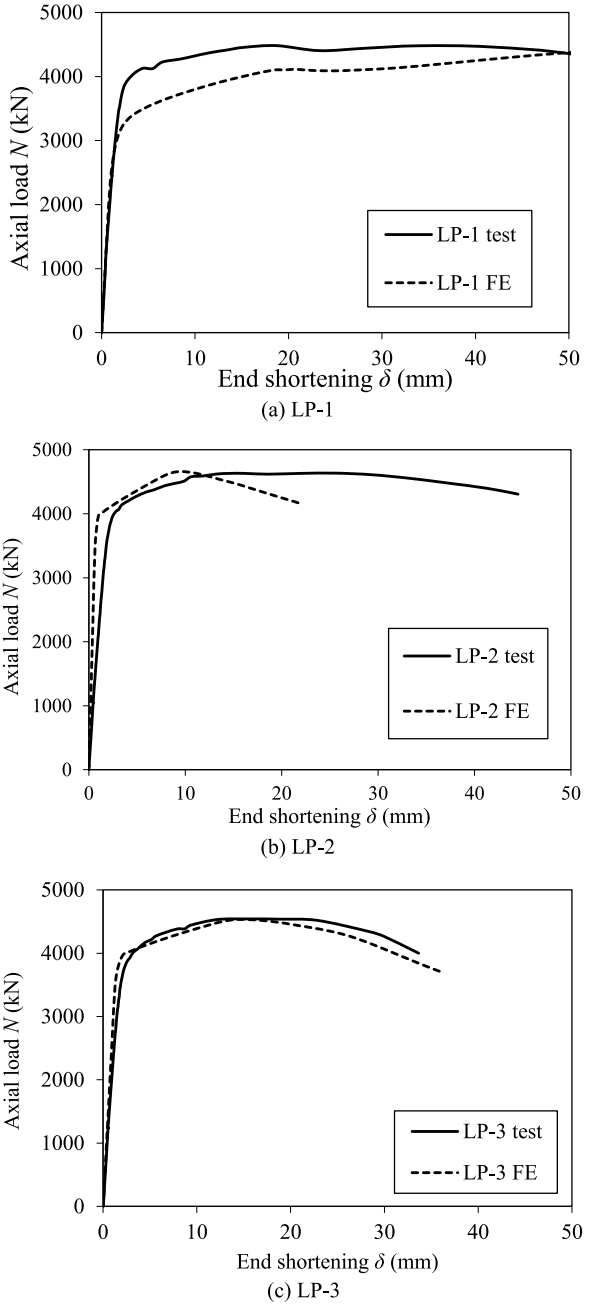

Fig. 15. Load-end shortening curves comparison.

4.3. Parametric study

The validated FE models are employed for a parametric investigation to add to the limited range of experimental design parameters and study the influence of various parameters on the ultimate capacity of lined pipes. A total of 62 FE models was analysed. Parameters of interests includes the outer pipe yield strength f_{yo}, the liner pipe proof strength f_{yi}, the contact pressure p_c induced by the residual hoop stress and the diameter to thickness ratio of the outer pipe. For each set of numerical investigations, the parameter of interests is changed while the rest parameters are set to the nominal value of the test specimens.

Firstly, various commonly used material properties of the outer and liner pipe were considered. The yield strength of the outer pipe f_{yo} was taken as 340, 440, 540 and 640 MPa and the 0.2% proof strength of the liner pipe f_{yi} was taken as 240, 350 and 420 MPa. The ultimate loads N_u are plotted in Fig. 17. It can be seen that increasing the strength of the outer pipe has a greater impact on the ultimate capacity, while the improvement from the liner pipe with a proof strength greater than 350 MPA can be ignored.

(a) LP-1

(b) LP-2

(c) LP-3

Fig. 16. Failure modes comparison.

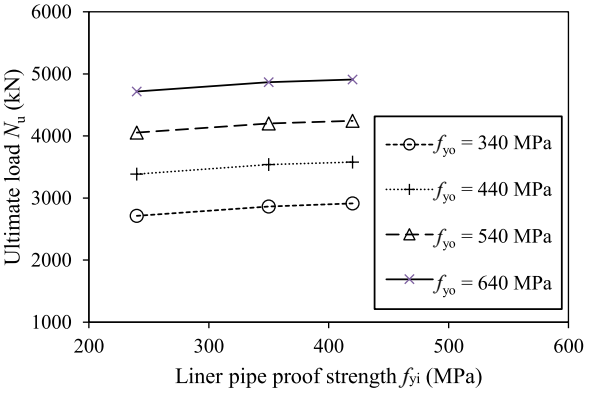

Fig. 17. Ultimate loads with various material properties.

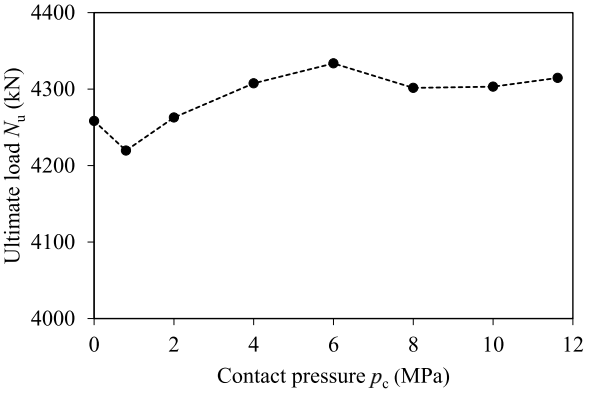

Fig. 18. Ultimate loads with various contact pressure.

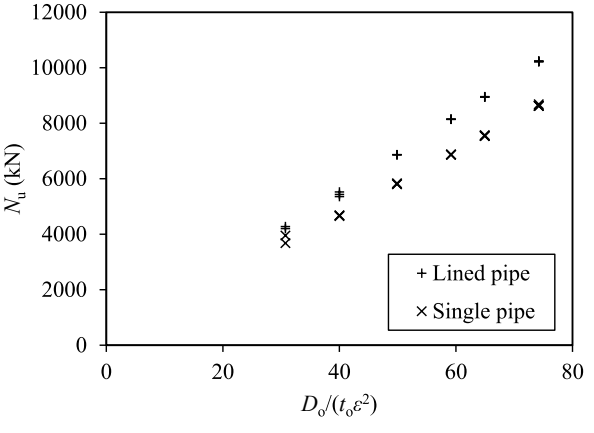

Fig. 19. Ultimate loads with various diameter-to-thickness ratios.

The second batch of parametric study focused on the influence of the contact pressure p_c between the liner and the outer pipe. Six contact pressure values were considered: 0, 0.8, 2, 4, 6, 8, 10 and 11.6 MPa. Noted that imperfection was not considered in this group of numerical analysis, since as shown by previous research [1], the difference on the ultimate capacities of stub columns with small initial imperfection or no imperfection is negligible. Similar to Ref. [2], the applied hoop stress and the contact pressure generated from the numerical models have a linear relationship, which can be explained by the load equilibrium of the cross-section. Fig. 18 summarises ultimate loads with various contact pressures. It can be seen that with an increasing contact pressure, the ultimate bearing capacities of lined pipes increase slightly from 4220 kN to 4333 kN, with an amplitude of 2.6% only.

Thirdly, different values of pipe diameters D were considered. Six commonly used diameters of the pipe D (16.3, 219.1, 273.1,

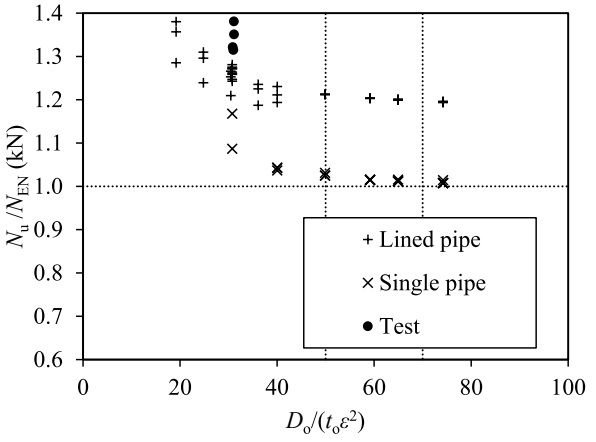

Fig. 20. Assessment of EN 1993-1-1 strength predictions.

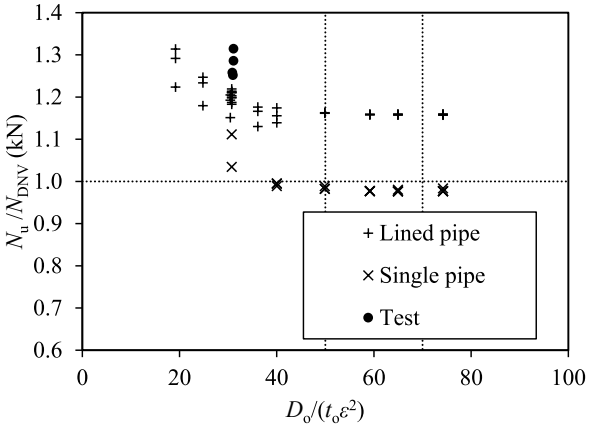

Fig. 21. Assessment of DNV–OS–F101 strength predictions.

323.9, 355.6, 406.4 mm) were selected to generate different cross-section classifications. The liner thickness of 3 mm and 0 mm was selected to consider lined pipes and single pipes, respectively. Different lengths of short lined pipes were also simulated for each cross-section and no clear difference was observed in the ultimate loads. Fig. 19 summarises the ultimate capacities of different diameter to outer pipe thickness ratios. It can be seen that with a higher diameter to thickness ratio there is a bigger enhancement of capacities from single pipes to lined pipes.

The results generated from all the parametric studies, together with the test results, are used to evaluate the existing design provisions, EN 1993-1-1 [21] and DNV–OS–F101 [22]. European code EN 1993-1-1 provides the general rules of steel structure design, in which the yield load is used to determine the ultimate strength of the outer pipe ($N_{EN} = A_o f_{yo}$) as stub columns. DNV–OS–F101 is generally employed to predict the ultimate strength of submarine pipeline and has been extensively adopted in engineering practices. The contributions by strain hardening properties to pipeline ultimate strength is reflected by a flow stress parameter a_c ($N_{DNV} = \alpha_c A_o f_{yo}$). Possible beneficial strengthening effect of liner on a steel pipe is not generally considered in engineering design.

The obtained test or FE to predicted results are plotted against the EN 1993-1-1 local slenderness parameter in Figs. 20 and 21, for EN 1993-1-1 and DNV–OS–F101, respectively, where the local slenderness parameter is $D_o/t_o\varepsilon^2$ and $\varepsilon=(235/f_{yo})$. The EN 1993-1-1 slenderness limits for Class 1 and 2 are also depicted. It may be concluded that the EN 1993-1-1 limits are safely applicable. Though in engineering practice the contribution of the liner to the ultimate strength is usually ignored, these figures show that the existence of linear pipe has significant enhancement on the bearing capacity. It can also be observed that all tested sections exceed their yield loads and this enhancement is more obvious with lower local slenderness. This is attributed to the significant strain hardening exhibited by stocky cross-sections, which is not accounted for in EN 1993-1-1. A proposal is therefore put forward employing the deformation based continuous strength method (CSM), which accounts for the strain hardening.

5. Proposal of ultimate strength calculation method

Having observed some inaccuracy in the strength predictions of the existing provisions, improvement is made in this new design

proposal. To rationally utilize the cross-sectional resistance contributed by the liner, the local buckling occurrence of the liner should be later than that of the outer pipe [1]. Therefore, a confinement factor ξ, which has been used extensively in design of concrete-filled steel tubular (CFST) structures [38–42] indicating the interaction behaviour between the outer steel tube and confined concrete, is introduced herein in the ultimate strength predictions. The superposition of the liner and the outer pipe strengths are subsequently allowed for ξ within a certain limit. Continuous strength method (CSM) which relates the cross-section resistance to the deformation capacity [23,24,43] is also incorporated herein to cover the design of submarine pipeline.

5.1. Confinement factor

The confinement factor ξ is defined in non-dimensional form as given in Eq. (3).

$$\xi = \frac{A_o f_{yo}}{A_i f_{yi}} \leq 6.0 \tag{3}$$

Wang et al. [1] suggested an upper limit of $\xi \leq 6.0$, where the liner was expected to fail beyond the local buckling of the outer pipe and the interaction behaviour between the components may further enhance the ultimate strength of the lined pipe. The ultimate strength of lined pipe N_{prop} can be calculated by superposing both the strengths of the outer pipe and liner as shown by Eq. (4),

$$N_{prop} = \begin{cases} N_{csm,o} + N_{csm,i}, \ for \ \xi \leq 6.0 \\ N_{csm,o}, \ for \ \xi > 6.0 \end{cases} \tag{4}$$

where $N_{\text{csm,o}}$ and $N_{\text{csm,i}}$ are the ultimate strengths of the outer and the liner pipe following the CSM calculation described in the next subsection. According to engineering practice, the application range is given as: outer piper yield stress $f_{\text{yo}} = 450$–600 MPa, liner yield stress $f_{\text{yi}} = 210$–480 MPa, outer pipe thickness $t_{\text{o}} = 6$–15 mm, liner thickness $t_{\text{i}} = 2.5$–4.0 mm, diameter to thickness ratio for both the outer pipe and liner $D/t = 15$–45.

5.2. Cross-sectional resistance

The cross-section resistances of both the outer and the liner pipe in compression are determined from the deformation capacity and material model from CSM, following the equations given in Ref. [24]. $N_{\text{csm,o}}$ and $N_{\text{csm,i}}$ can be calculated separately by their geometry and material properties.

The local cross-section slenderness is defined through Eq. (5),

$$\overline{\lambda_c} = \sqrt{\frac{f_y}{f_{cr}}} \tag{5}$$

where f_{cr} is the elastic critical buckling stress and is calculated by Eq. (6) for a circle hollow section under compression.

$$f_{cr} = \frac{E}{\sqrt{3(1-\nu^2)}} \frac{2t}{D} \tag{6}$$

A continuous relationship between the local cross-section slenderness and deformation capacity has been developed in CSM. The deformation capacity is represented by the strain ratio ($\varepsilon_{\text{csm}}/\varepsilon_{\text{y}}$) and taken as the strain at ultimate strength ε_{csm} normalized by the yield strain ε_{y}. The strain ratio can be calculated by Eq. (7) for non-slender and slender sections, with the upper limits determined by material ductility and strain hardening.

$$\frac{\varepsilon_{csm}}{\varepsilon_y} = \begin{cases} \dfrac{4.44 \times 10^{-3}}{\overline{\lambda_c}^{4.5}}, & for \ \overline{\lambda_c} \leq 0.3 \ but \ \dfrac{\varepsilon_{csm}}{\varepsilon_y} \leq min\left(15, \ \dfrac{C_1 \varepsilon_u}{\varepsilon_y}\right) \\ \left(1 - \dfrac{0.224}{\overline{\lambda_c}^{0.342}}\right) \dfrac{1}{\overline{\lambda_c}^{0.342}}, & for \ 0.3 < \overline{\lambda_c} \leq 0.6 \end{cases} \tag{7}$$

where C_1 is the material coefficient and ε_{u} is the strain at ultimate tensile stress of the material.

The CSM limiting stress f_{csm} is defined in Eq. (8).

$$f_{csm} = \begin{cases} f_y + E_{sh}\varepsilon_y \left(\dfrac{\varepsilon_{csm}}{\varepsilon_y} - 1\right), \ for \ \dfrac{\varepsilon_{csm}}{\varepsilon_y} \geq 1 \\ E\varepsilon_{csm}, \ for \ \dfrac{\varepsilon_{csm}}{\varepsilon_y} < 1 \end{cases} \tag{8}$$

where E_{sh} is the strain hardening modulus for an elastic, linear strain hardening material model. Noted that both stainless steel and carbon steel have been included in the CSM by using different material models.

The CSM cross-sectional compression resistance can be calculated by Eq. (9).

Table 6
Comparison of the proposed design method and existing design predictions.

No. of test: 4 No of FE:41	N_u/N_{pred}		
	N_u/N_{prop}	N_u/N_{EN}	N_u/N_{DNV}
Mean	1.052	1.244	1.164
COV	0.064	0.043	0.042

$$N_{csm} = \begin{cases} Af_{csm}, \ for \ \overline{\lambda_c} \leq 0.3 \\ \dfrac{\varepsilon_{csm}}{\varepsilon_y} Af_y, \ for \ 0.3 < \overline{\lambda_c} \leq 0.6 \end{cases} \tag{9}$$

5.3. Assessment of the proposed design method and reliability analysis

The experimental and numerical results for lined pipes obtained in this study with the collected experimental result from previous research [19] were used to assess the predictions from the proposed method and the current design codes EN 1993-1-1 [21] and DNV–OS–F101 [22]. The dataset consists of three test results from this study, one from Focke et al. [19] and 41 numerical results of lined pipes from this study. The mean values and COVs of the test/FE results to predicted capacities N_u/N_{pred} ratios are listed in Table 6. The mean ratios of N_u/N_{pred} are equal to 1.052, 1.244 and 1.164, for the proposal Eurocode and DNV code, respectively, with corresponding COVs equal to 0.064, 0.043 and 0.042. It can be seen that the proposal offers significant improvement on ultimate strength prediction accuracy, while the predictions are still within conservative range.

6. Conclusions

A comprehensive investigation focusing on the interaction of the lined pipes under axial compression has been undertaken. The following conclusions can be drawn:

Saw tests and ring-split tests were carried out to measure the axial and radial interaction between the liner and the outer pipe. It was found that the residual axial stress was especially lower after reeling and the residual hoop stress was compressive in the liner and tensile in the outer pipe, both at a low stress level.

Short lined pipe ultimate strength tests were carried out and the development of liner wrinkle was captured by a built-in camera. The experimentally captured loading and strain histories, failure modes and ultimate strengths were compared with the numerical analyses and predictions from the current engineering practice. The importance of the liner contribution and material strain hardening feature in the structural response of specimens have been highlighted in this paper.

Base on the test results and supplementary numerical simulations, a new cross-sectional ultimate strength calculation method was proposed to rationally exploit the liner structural resistance and the material strain hardening. A confinement factor limit was introduced to ensure the rational consideration of the liner. The continuous strength method initially developed for stocky tubular steel structures were extended to cover the design of lined pipes. The comparisons with the conducted and collected data showed that the proposed design method provided improved prediction accuracies on the ultimate strength.